CRYSTAL GROWTH & DESIGN

Article

Kinetics and Thermodynamics of Glucose Isomerase Crystallization

Mike Sleutel, Ronnie Willaert, Christopher Gillespie, Christine Evrard, Lode Wyns, and Dominique Maes

Cryst. Growth Des., **Article ASAP**

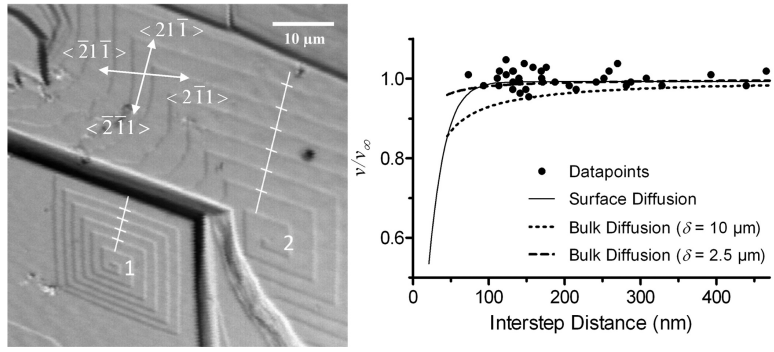

More About This Article

Additional resources and features associated with this article are available within the HTML version:

- Supporting Information
- Access to high resolution figures
- Links to articles and content related to this article
- Copyright permission to reproduce figures and/or text from this article

View the Full Text HTML

Crystal Growth and Design is published by the American Chemical Society. 1155 Sixteenth Street N.W., Washington, DC 20036

CRYSTAL GROWTH & DESIGN
XXXX
VOL. XXX, NO. XX

Kinetics and Thermodynamics of Glucose Isomerase Crystallization

Mike Sleutel,*,† Ronnie Willaert,† Christopher Gillespie,§ Christine Evrard,‡ Lode Wyns,† and Dominique Maes†

Structural Biology Brussels, Flanders Interuniversity Institute for Biotechnology (VIB), Vrije Universiteit Brussel, Belgium, Laboratoire de Biologie Moleculaire et de Genie Genetique, Universite de Liege, Belgium, and Department of Chemical Engineering, Center for Molecular and Engineering Thermodynamics, University of Delaware, 150 Academy Street, Newark, Delaware 19176

Received July 14, 2008; Revised Manuscript Received October 6, 2008

ABSTRACT: A quantitative study using laser confocal microscopy combined with differential interference microscopy on the kinetics and thermodynamics of the crystallization of glucose isomerase is presented. Fundamental crystallization parameters are determined from the kinetics of step advancement and rates of two-dimensional (2D) nucleation. The ruling mass transfer pathway and accompanying activation barriers are discussed. In brief, the solubility exhibits normal temperature dependence and the crystallization enthalpy is the thermodynamic driving force. The diminishing entropic cost for higher PEG concentrations is attributed to water structuring and a decrease in water activity. The prominent step generation mechanism is homogeneous 2D nucleation for high supersaturations. At low driving forces 2D nucleation occurs on anomalously hyperactive sites and the step edge free energies for homogeneous and heterogeneous nucleation are determined. The number of nucleation centers for both mechanisms are estimated and from the density of nucleation centers we obtain for the activation barrier of adsorption $\sim$3.8 kJ mol^{-1}. No step-step interaction is observed for interstep distances >70 nm. Theoretical fits of step velocity data suggest surface diffusion makes a non-negligible contribution to surface kinetics. From the temperature dependence of the step kinetic coefficient the activation barrier for crystallization was determined to be <22.4 kJ mol^{-1}.

Introduction

The crystal habit is (initially) composed of three types of crystal faces, that is, facetted (F), stepped (S), and kinked (K) faces.[1] The latter two grow much faster due to their abundance of growth sites, that is, kinks, and as such disappear during the course of the growth process, leading to a crystal habit outlined by singular F faces. Under conditions of a nonvanishing activation barrier for nucleation and kink formation (i.e., below the kinetic roughening transition[2] and with moderate molecular thermal energy,[3] that is, below the thermal roughening temperature) these interfaces are smooth surfaces where the relatively rare incorporation sites are situated along the molecular rows that define the edges of the unfinished advancing crystalline layers traversing the surface. For F faces where kinks are typically widely spaced, an interesting competition between mass transfer through bulk and surface diffusion arises. With the presence of kink-free terraces in between the (linear) sinks, that is, steps, the growth units can now also adhere to the surface, diffuse two-dimensionally and incorporate into kinks, a pathway previously not possible on the S and K faces in the early stages of crystal growth. Systems where the intersink distance becomes far greater than the molecule size may benefit from a reduction in dimensionality in terms of trapping efficiency of growth units. For instance, Adam and Delbrück showed[4,5] that the efficiency of biological diffusion processes such as membrane-associated reactions can be increased by confining the search space of diffusing species from the surrounding bulk liquid phase to a two-dimensional surface. They considered the specific case of bacterial chemotaxis where, not very much unlike crystallization, substrates can reach specific sinks (receptor molecules) through either bulk diffusion or sequential adsorption followed by surface diffusion. Elaborating on this notion, Berg and Purcell[5] found that the mass transfer efficiency of 2D diffusion depends on the average distance between sinks on the surface, with *sinks* being kinks in our case, or more generally, steps. It is not inconceivable that a similar mechanism may operate for the crystallization case.[6] Of course, the ruling mass transfer pathway will not be defined solely by the relative pathway efficiencies, but to a great extent by the heights of the activation barriers the molecules encounter.

Initially, the surface diffusion mechanism for solution growth was considered to be improbable given the small energy of dissolution and the large diffusivity of proteins in the bulk. The absence of experimental data on step diffusion field overlap strengthened this notion. This is not surprising considering that typical diffusion length scales (commensurate with the mean free path of the admolecules) have been estimated to be as low as 50−500 nm, or 10−100 molecule diameters, which is smaller than typical interstep distances for the conditions utilized in most studies. A shift in the direct incorporation paradigm came about by both Michaelson interferometry and atomic force microscopy experiments from which the existence of step-step interaction as a consequence of surface diffusion field overlap and step decoupling through the Schwoebel effect was demonstrated for the crystallization from solution of both small molecules (ADP[7]) and proteins (lysozyme,[8] canavalin,[9] insulin[10]). Additional evidence supporting the surface diffusion mechanism was found in the molecular-scale incorporation statistics at the kink level ((apo)ferritin,[11] triose phosphate isomerase[12]) and more recently[13] through single-molecule visualization of fluorescent labeled molecules at the solution−crystal interface (F-HEWL). In contrast, the role of surface diffusion on step kinetics on the (010) face of lysozyme was deemed negligible[14] given the low terrace coverage of adsorbed molecules. Given that (in)direct evidence for the surface diffusion mechanism has been presented for five proteins only, it can hardly be considered a universal trait of macromolecular crystallization. Also, the scarcity of

* To whom correspondence should be addressed. E-mail: mike.sleutel@vub.ac.be. Telephone: +32-2-6291923. Fax: +32-2-6291963.
† Vrije Universiteit Brussel.
§ University of Delaware.
‡ Universite de Liege.

10.1021/cg800756h CCC: $40.75

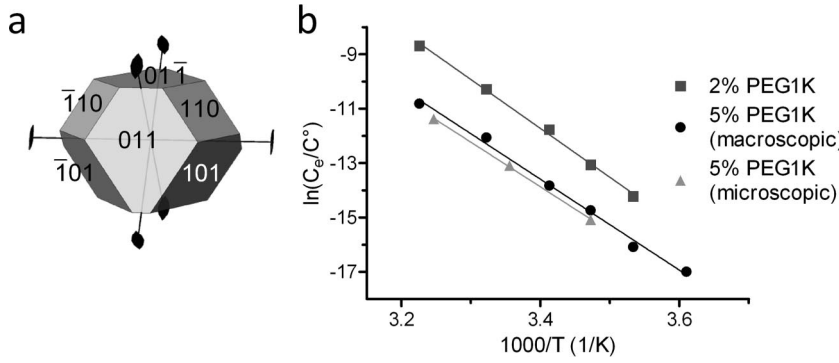

Figure 1. (a) Orthorombic (*I*222) glucose isomerase crystal (nine faces), habit is defined by planes with indexes {011}, {101}, and {110}. (b) van't Hoff plot of the solubility data based on batch method (gray squares 2% PEG 1000 and black circles 5% PEG 1000) and zero step velocity method (light gray triangles 5% PEG); lines indicate fits based on eq 3.

quantitative data on the various activation barriers determining the rates of step advancement exemplifies the need for more research on this topic. Hence, we present in this work additional evidence in support of the surface diffusion hypothesis for the crystallization of macromolecules. We study the specific case of glucose isomerase. In the first section we address the thermodynamics of crystallization, followed by two quantitative sections on the anisotropy of surface kinetics and the mechanism of 2D nucleation. In the fourth and fifth parts of this work, we discuss the ruling mass transfer pathway (i.e., surface diffusion) and the accompanying activation barriers for the elementary surface processes.

Materials and Methods

Crystallization of Glucose Isomerase. Glucose isomerase from *Streptomyces rubiginosus* was purchased from Hampton Research (California, USA). The protein solution was dialyzed against 10 mM Hepes buffer pH 7.0 and 1 mM $MgCl_2$. Protein concentrations were determined by UV absorbance at 280 nm. For the atomic force microscopy (AFM) experiments, crystals were grown at 20 °C on nonsiliconized 10 mm diameter glass discs using the sitting drop vapor diffusion technique with the aid of microbridges (Hampton Research). The protein solution used in the crystallization set-ups contained 30 mg/mL protein in 100 mM Hepes pH 7.0 and 200 mM $MgCl_2$. Drops were prepared by mixing 2 μL of glucose isomerase solution with 2 μL reservoir solution of 100 mM Hepes pH 7.0, 200 mM $MgCl_2$, and 5% PEG 1000. For the laser confocal microscopy experiments, crystals were grown in situ using the batch method at 30 mg/mL glucose isomerase, 100 mM Hepes pH 7.0, 200 mM $MgCl_2$, and 5% PEG1000. At these conditions, the protein crystallizes in the orthorhombic form (*I*222, $a = 94.01$ Å, $b = 99.37$ Å, $c = 103.01$ Å).[15]

Solubility Curve Determination. Crystals were grown using the batch method in eppendorf tubes and stored for one month at various temperatures, that is, 277, 283, 288, 293, 301, and 310 K. Rigorous mixing of samples was performed at weekly intervals to avoid premature cessation of growth as a consequence of impurity surface poisoning. After one month, samples were centrifuged for 30 min at 8000 rpm at their respective incubation temperatures. Protein concentration of the obtained supernatant was taken to be the equilibrium concentration for the respective condition.

Ideality Assumption. To verify the validity of the ideality assumption ($\gamma_e = 1$) we calculate the activity coefficient γ_e using[16] $\ln \gamma_e = 2B_2MC_e$ where M is the molecular mass of glucose isomerase, B_2 is the second virial coefficient and C_e the equilibrium protein concentration. Since the value of B_2 for glucose isomerase is not available, we employ a lower limit B_2, that is, the lowest value present in the literature -8×10^{-4} cm^3 mol g^{-2} for protein crystallization. Using this lower limit we then obtain a non-negligible maximum error of 19% for the determination of the standard entropy $\Delta S°$ and enthalpy $\Delta H°$ of crystallization. Since nonideality ($\gamma_e \neq 1$) is more pronounced for higher protein concentrations,[17] we omit the highest C_e (310 K) in the determination of $\Delta H°$ and $\Delta S°$ to lower the introduced error. The linear fit of the truncated data set (277−301 K) then yields an admissible error of ± 6% for the determination of the thermodynamic parameters and $\gamma_e = 1$ becomes justified.

Surface Imaging Using Laser Confocal Microscopy (LCM) Combined with Differential Interference Contrast Microscopy (DIM). Growing (011) faces of orthorhombic glucose isomerase crystals were observed in situ by LCM-DIM. For this, a D-Eclipse C1 confocal system was attached to an inverted Eclipse TE-2000 U optical microscope (Nikon, Brussels, Belgium). An air objective lens PlanFluor 20× with a numerical aperture of 0.45 and a working distance of 7.6 mm was used (theoretical lateral resolution 660 nm). The diameter of the confocal aperture used for the observation was 103 μm. A Nomarski prism was inserted into the optical path to utilize differential interference contrast. The experimental cell was a 45 mm × 12.5 mm quartz cuvette with two detachable windows (Hellma, Müllheim, Germany). Crystals were illuminated with an argon-ion laser with a wavelength of 488 nm. Photomicrographs of 512 × 512 pixels were acquired over a 4 s scan time with a pixel-dwell of 11 μs. For the conditions used in this study, glucose isomerase crystallizes exclusively in the orthorhombic form (*I*222) (Figure 1a). For this polymorph, the crystal habit is defined by planes with indexes {011}, {101}, and {110}. After nucleation inside the experimental cell, the four crystallographically equivalent (011), ($0\bar{1}1$), ($01\bar{1}$), and ($0\bar{1}\bar{1}$) prism faces ({011}) were most frequently parallel to the plane of observation of the LCM-DIM experiment and hence were studied in this work.

Atomic Force Microscopy (AFM). AFM imaging of the crystallization processes was conducted in tapping mode using Nanoscope IIIa multimode AFM (Veeco, Santa Barbara, USA). Standard silicon nitride and oxide sharpened SPM tips (Veeco, Santa Barbara, USA) were used. Cantilevers with nominal force constants of 0.01 N/m were typically utilized. In order to minimize the force applied to the crystalline surface during scanning, the set point voltage was continually adjusted to the lowest level for which tip-crystal contact was maintained. Step growth velocities were determined by scanning perpendicular to the step and disabling the slow scan (vertical) axis. The slopes of the steps were taken as the tangential growth velocities.

Results and Discussion

Crystallization Thermodynamics Are Characterized by a Negative Enthalpy Contribution. The protein solubility C_e dependence on temperature was measured between 277 and 310 K for the condition 100 mM Hepes pH 7.0, 200 mM $MgCl_2$, 2% and 5% PEG 1000. C_e was determined macroscopically by measuring the protein concentration C of the bulk solution in equilibrium with the solid crystalline phase (Figure 1b black circles and gray squares, macroscopic) and microscopically by determining the protein concentration for which the step velocity is zero (Figure 1b light gray triangles, microscopic). As can be seen from Figure 1b, glucose isomerase exhibits a normal solubility dependence of temperature for PEG1000, that is, protein solubility increases with temperature. This solubility data

Table 1. Standard Free Energy of Crystallization as Function of Temperature

	ΔG°_{cryst} (kJ mol^{-1})[a]	
T (K)	2%	5%
277	−39	
283	−38	−33
288	−35	−31
293	−34	−29
301	−30	−26
310	−28	−22

ΔH°_{cryst} (kJ mol^{-1})[a]	
2%	5%
−156 ± 6	−145 ± 7
ΔS°_{cryst} (kJ mol^{-1})[a]	
2%	5%
−435 ± 25	−380 ± 22

[a] Based on batch method.

can be used to characterize the thermodynamics of crystallization using the expression for the standard free energy of crystallization ΔG° and the equilibrium constant of crystallization K_{cryst}[18]

$$\Delta G^\circ = \Delta H^\circ - T\Delta S^\circ = -RT \ln K_{cryst} \quad (1)$$

$$K_{cryst} = a_e^{-1} = \left(\gamma_e \frac{C_e}{C^\circ}\right)^{-1} \approx \left(\frac{C_e}{C^\circ}\right)^{-1} \quad (2)$$

where ΔH° and ΔS° are the standard enthalpy and entropy of crystallization, respectively, T is the temperature, $R = 8.314$ J mol^{-1} K^{-1} is the universal gas constant, a_e is the activity of glucose isomerase in solution in equilibrium with the crystal, γ_e is the corresponding activity coefficient, C_e is the equilibrium protein concentration and $C^\circ = 1$ mol kg^{-1} the concentration of the solution in the chosen standard state. Note that the right part of eq 2 assumes solution ideality, that is, $\gamma_e = 1$ (for justification, see Materials and Methods). From eqs 1 and 2 it follows that

$$\ln\left(\frac{C_e}{C^\circ}\right) = \frac{\Delta H^\circ}{RT} - \frac{\Delta S^\circ}{R} \quad (3)$$

where ΔH° and ΔS° can be obtained from the slope (van't Hoff relation) and intercept, respectively, of the linear curve displayed in Figure 1b. The linear feature of the obtained van't Hoff plot implies that ΔH° is temperature independent for the sampled temperature range. The linear fit gives for 2% PEG $\Delta H^\circ_{cryst} = -156 \pm 6$ kJ mol^{-1} and for $\Delta S^\circ_{cryst} = -435 \pm 25$ J mol^{-1} K^{-1}. For 5% PEG we obtain $\Delta H^\circ_{cryst} = -145 \pm 7$ kJ mol^{-1} and for $\Delta S^\circ_{cryst} = -380 \pm 22$ J mol^{-1} K^{-1} (see Table 1). The negative entropy contribution indicates entropy loss upon the attachment of protein molecules to the crystal either due to constrained translational and rotational degrees of freedom[19] and due to the trapping or rearrangement of water[20,21]/PEG[22−25] molecules in the crystal lattice. The entropy change thus disfavors crystallization. The combined entropy balance (loss of translational, rotational and gain of vibrational degrees of freedom) due to the ordering of proteins in the bulk lattice was estimated to be[26] from –100 to –280 J mol^{-1} K^{-1}, which is significantly smaller than the value obtained in this study. Hence, the negative entropic contribution is possibly enlarged even more by the trapping of water or solvent molecules. Note that there is a significant difference in ΔH°_{cryst} and ΔS°_{cryst} between 2% and 5% PEG 1000. A possible explanation may lie in the activity of the bulk water as suggested in ref 27. As the PEG concentration increases, the viscosity and the overall number of water molecules bound to PEG increases (∼75 water molecules/PEG 1000[28]) and the bulk water activity decreases.[29] Hence, the entropy of the water molecules in the liquid phase decreases. The entropic cost of water/solute trapping therefore becomes less high. For crystallization to occur, this entropy contribution needs to be compensated, however. For the temperature range selected in this study, the opposing entropic effect is indeed counteracted and surpassed by the negative sign and magnitude of the enthalpic change, indicating an exothermic crystallization (i.e., heat is released during crystallization) making the process thermodynamically permissible.

For the C_e data obtained by the zero step velocity method (microscopic) for the $<2\bar{1}1>$ direction on the (011) face with 5% PEG 1000, $\Delta H^\circ_{step} = -136 \pm 3$ kJ mol^{-1} and $\Delta S^\circ_{step} = -490 \pm 110$ J mol^{-1} K^{-1}. These values are relatively similar to the values obtained with the (macroscopic) batch method. Also, ΔH°_{cryst} and ΔS°_{cryst} differ roughly 10% with the values obtained for the precipitant ammonium sulfate,[30] which suggests enthalpy and entropy are relatively constant for the two precipitants. A similar invariability has also been observed for the crystallization of lysozyme.[21]

Combining eqs 1 and 2 gives $\Delta G^\circ = RT \ln(C_e/C^\circ)$, allowing the evaluation of ΔG° using the data in Figure 1b. The results are summarized in Table 1. The observed decrease in absolute ΔG° as a function of temperature is the result of the increasing contribution of $T\Delta S^\circ$ component, gradually impeding crystallization. These values are comparable to ΔG° for other proteins,[21] for example, apoferritin, CO-hemoglobin C, and lysozyme, respectively, −42, −25, and −16 kJ mol^{-1}.

Step Growth Kinetics Are Anisotropic. For the tested supersaturation range $\sigma = \ln(C/C_e) = 0.3 - 5.0$ the dominating step generating mechanism on the (011) face is two-dimensional (2D) nucleation (Figure 2a). For $\sigma > 5.0 \pm 0.1$ at 293 K, the (011) face undergoes a roughening transition and continuous growth is the dominating growth mechanism.[31] For low supersaturation, growth hillocks have been observed only sporadically in this study (Figure 2a). Foreign macroparticles ($\pm 10\ \mu$m) were observed underneath the edge dislocation (data not shown) suggesting that impurity or mother liquor trapping[32] is a dislocation generating mechanism for glucose isomerase.

To orient the surface coordinate system, we note that the steps outlining the 2D islands are parallel to the crystal's edges (defined by zones $[\bar{1}\bar{1}1]$, $[\bar{1}1\bar{1}]$, $[1\bar{1}1]$, and $[11\bar{1}]$). This indicates that the steps are oriented along the molecular rows in the crystal, that is, they are limited by closest packed directions. The rhombic and polygonal shape of the 2D islands and the spiral, respectively, reflect the anisotropy of the step growth kinetics. Step velocity is maximal in the direction of the vertices of the rhombic islands. Evidence for step growth anisotropy is also found in the step density of the four vicinals of spiral growth pyramids. Step densities are higher in the $<\bar{2}\bar{1}1>$ and $<\bar{2}1\bar{1}>$ direction indicative of growth rate anisotropy.[33,10] To quantify the anisotropy in incorporation kinetics, the tangential step velocity v_{step} dependence on $C - C_e$ for the four crystallographic directions $<\bar{2}\bar{1}1>$, $<2\bar{1}1>$, $<21\bar{1}>$, and $<\bar{2}1\bar{1}>$ perpendicular to the crystal's edges were determined at 288 K. A linear relationship between v_{step} and $C - C_e$ is found (Figure 2b), indicating a high kink density. We interpret these data using $v_{step} = \Omega\beta_{step}(C - C_e)$,[34] yielding $\beta_{<2\bar{1}1>} = 2.5 \pm 0.2 \times 10^{-4}$ cm/s, $\beta_{<\bar{2}\bar{1}1>} = 4.6 \pm 0.2 \times 10^{-4}$ cm/s, $\beta_{<\bar{2}1\bar{1}>} = 4.4 \pm 0.4 \times 10^{-4}$ cm/s, and $\beta_{<21\bar{1}>} = 3.1 \pm 0.2 \times 10^{-4}$ cm/s. The ratio $\beta_{<2\bar{1}1>}/\beta_{<\bar{2}\bar{1}1>}/\beta_{<\bar{2}1\bar{1}>}/\beta_{<21\bar{1}>} \approx 1.0/1.8/1.8/1.2$ demonstrates the presence of significant anisotropy in step incorporation kinetics. The same anisotropy is reflected in the step density n of the four vicinal slopes of the spiral hillock in Figure 2c, $n_{<2\bar{1}1>}/$

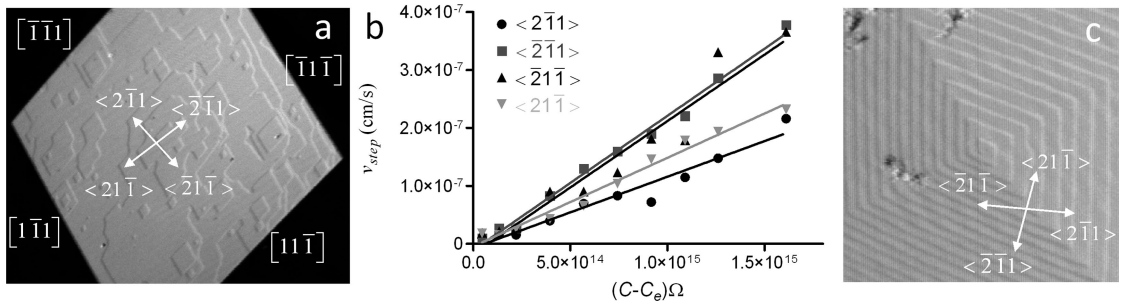

Figure 2. (a) 2D nucleation on the (011) face of an orthorhombic glucose isomerase crystal: miller indices within square brackets denote crystal edge orientation, miller indices within angular brackets denote directions perpendicular to crystal's edges. (b) v_{step} as function of driving force: slopes of the linear fits yield the step kinetic coefficient β_{step} for the four directions, (c) growth hillock spiraling around an edge dislocation protruding the (011) face, foreign particles present in the crystal bulk or on the surface can be seen.

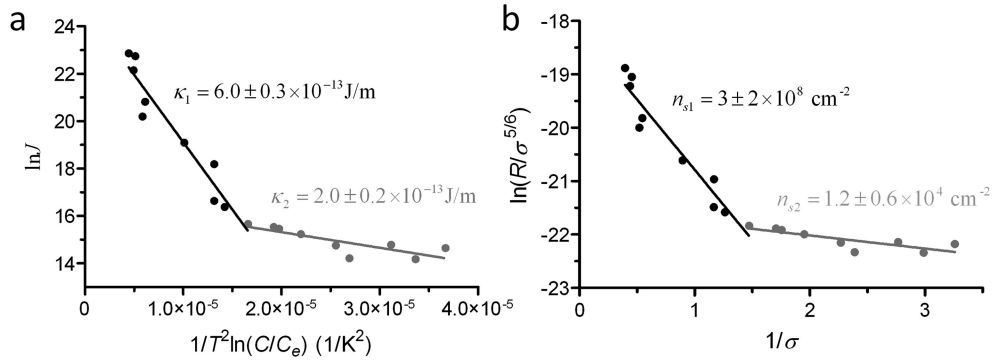

Figure 3. (a) 2D nucleation rates as a function of $1/T^2$ ln(C/C_e). Solid lines represent fits based on eq 4. Two domains are clearly discernible: homogeneous nucleation at $\sigma > 0.7$ (black dots), heterogeneous nucleation at $\sigma < 0.7$ (gray dots). (b) Supersaturation dependence of the normal growth rate R produced by 2D nucleation. Solid lines represent fits based on eq 6.

$n_{<\bar{2}1\bar{1}>}/n_{<\bar{2}1\bar{1}>}/n_{<21\bar{1}>} \approx 1.0/1.7/1.8/1.2$. Note that spiral anisotropy (degree of polygonization) is determined by both the anisotropy of the step line energy and of the step kinetic coefficient. While the former dominates in the center of the spiral, anisotropy in β becomes pronounced at the spiral's periphery.[33] Hence, we conclude from the polygonal step shape near the spiral's center and at the spiral's periphery (Figure 2c) that the step line energy contains the same anisotropy as β.

Heterogeneous 2D Nucleation Is the Prominent Step Generation Mechanism at $\sigma = \ln(C/C_e) \leq 0.7$. While 2D nucleation is the dominating step generation mechanism at $0.3 < \sigma < 5.0$ for the (011) crystal face of *undisturbed* crystals (i.e., no incorporation of microcrystals, no mechanical stress), we observed spiral dislocations only sporadically. However, the occurrence of growth hillocks was significantly higher for *disturbed* crystals. A similar observation has also been made for lysozyme[35] where multiple nucleation on dislocation-free crystals was observed. To study the kinetics of step generation more quantitatively, we measured the 2D nucleation rates as a function of protein concentration (Figure 3a). The steady-state 2D nucleation rates J were evaluated using a model derived from classical nucleation theory.[1]

$$\ln J = \ln(\omega^*\Gamma Z) - \frac{\pi\kappa^2 s}{k^2T^2\ln(C/C_e)} \qquad (4)$$

where ω^* is the frequency of attachment of molecules to the critical 2D nucleus, Γ is the Zeldovich factor, Z is the steady-state admolecule surface concentration, κ is the specific edge free energy and s is the surface area of a single molecule in the critical 2D nucleus (determined using AFM: $\pm 9.7 \times 10^{-17}$ m^2). From Figure 4a we see that ln J follows a clear linear relationship as a function of $1/T^2$ ln(C/C_e) with a kink around 1.66×10^{-7} K^{-2}, being ln(C/C_e) = 0.7 at 293 K. Such a kink has been observed for thaumatin,[36] lysozyme,[35] and inorganic crystals of ADP[37] and can interpreted as homogeneous and heterogeneous nucleation at high (regime 1) and low (regime 2) supersaturations, respectively. The slower decrease in ln J (larger slope) for $\sigma > 0.7$ indicates a smaller specific edge free energy that stems from 2D nucleation on hyperactive sites such as defects and impurity particles. Fits based on eq 4 of the two linear regimes in Figure 3a yield $\kappa_1 = 6.0 \pm 0.3 \times 10^{-13}$ J/m and $\kappa_2 = 2.0 \pm 0.2 \times 10^{-13}$ J/m. The two-dimensional analog of κ, that is, the effective surface free energy of the step end α, can be estimated using $\alpha = \kappa/h$[35] (the step height $h \approx 7$ nm determined using AFM), giving for $\alpha_1 = 0.086 \pm 0.004$ mJ/m^2 and $\alpha_2 = 0.029 \pm 0.003$ mJ/m^2, respectively. These values are 1 order of magnitude smaller than for lysozyme[35] and 3−4 times smaller than for catalase[38] and thaumatin[36] and are commensurate with the measured high 2D nucleation rates for this case.

From the steady-state 2D nucleation rates combined with the knowledge of the step kinetic coefficient, we calculate the supersaturation dependence of the normal growth rate R using the birth and spread model[33]

$$R \simeq h(\pi v_{step}^2 J)^{1/3} = h[\pi(\Omega\beta_{step}(C - C_e))^2 J]^{1/3} \quad \text{if } S^{1/2} > (v_{step}/J)^{1/3} \qquad (5)$$

where S is the surface area of the crystal face. Typical crystal length scales were 50 μm, which is significantly larger than the maximal value of $(v_{step}/J)^{1/3}$ achieved in this study, that is, ± 10 μm. Hence, the use of eq 5 is justified. Expressing the normal growth rate in the coordinates $\ln(R/\sigma^{5/6})$ versus $1/\sigma$ allows for

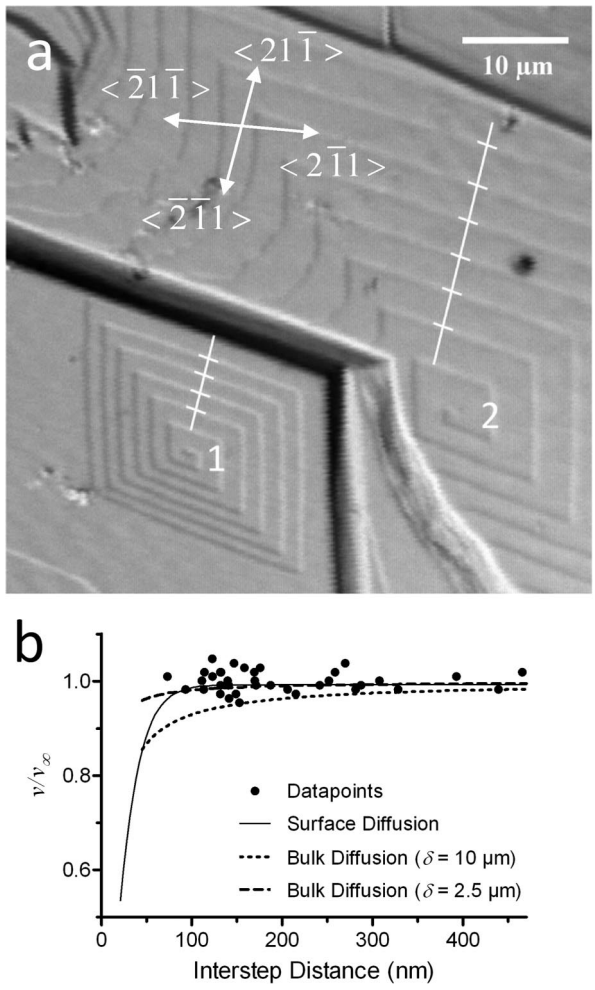

Figure 4. (a) Two spiral dislocations on the (011) face with single (1) and double (2) Burgers vector. White lines illustrate the difference in interstep distance; (b) step velocity dependence on interstep distance measured with AFM, fit based on surface diffusion model (solid line, $D_{sd} = 10^{-11}$ cm^2/s) and on bulk diffusion model (dashed line, $\delta = 2.5$ μm; dotted line, $\delta = 10$ μm).

the determination of the number of 2D nucleation centers n_s using[37]

$$\ln(R/\sigma^{5/6}) = \ln[hC_e\beta_{step}(\Omega^2 h a n_s)^{1/3}] - \frac{\pi\Omega\alpha^2 h}{3(kT)^2\sigma} \qquad (6)$$

with a being the distance between adjacent molecules (determined using AFM: 9−10 nm). From the slope of the linear fit in Figure 3b one can determine the effective surface free energy α. For the regions of homogeneous and heterogeneous nucleation we obtain, respectively, $\alpha_1 = 0.110 \pm 0.005$ mJ/m^2 and $\alpha_2 = 0.034 \pm 0.005$ mJ/m^2. Note that these values are quite comparable to the values obtained from the fits based on eq 4, hereby validating the applicability of the birth and spread model.

Extrapolation of the linear fits presented in Figure 3b gives the intercept with the ordinate axis, which in its turn yields $n_{s1} = 3 \pm 2 \times 10^8$ cm^{-2} for the regime of homogeneous nucleation. For lower supersaturations where nucleation is assumed not to occur around *native* admolecules but at anomalously active sites (e.g., impurity particles), we get for the surface concentration of active sites $n_{s2} = n_s^* = 1.2 \pm 0.6 \times 10^4$ cm^{-2}. These values are quite similar as obtained for thaumatin[36] and ADP.[37]

Steps Do Not Interact above Interstep Distances of 70 nm. Figure 4a shows a LCM-DIM image of two growth hillocks with opposite sign spiraling around two edge dislocations protruding the (011) crystal surface. The interstep distances λ_i of the four vicinal slopes of both spirals were measured and the following ratios were calculated $L_i = \lambda_i^{(2)}/\lambda_i^{(1)}$, where the superscripts denote spiral 2 and 1 and the subscripts denote the crystallographic direction. This gives $L_{<2\bar{1}1>} = 2.0 \pm 0.3$, $L_{<\bar{2}1\bar{1}>} = 1.9 \pm 0.2$, $L_{<\bar{2}1\bar{1}>} = 1.8 \pm 0.2$ and $L_{<21\bar{1}>} = 2.0 \pm 0.1$, that is, the interstep distance for spiral 2 is twice as for spiral 1. The spacing λ between two successive steps of a polygonized spiral with 4-fold symmetry is determined by the step free energy and the supersaturation through[39,40,1]

$$\lambda \approx 8\rho_c = 8\frac{2b\kappa a^2}{kT\sigma} \qquad (7)$$

where ρ_c is the critical length of a polygonized square 2D nucleus and b is the spirals Burgers vector perpendicular to the surface. Assuming a constant supersaturation and using eq 7 we can ascribe a simple single and double Burgers vector to spiral 1 and 2, respectively. Because of the lateral resolution of this technique (± 0.6 μm) the individual steps of spiral 2 cannot be resolved. Also, we observed no decoupling of steps from spiral 2. From a 56 min time-lapse movie of the area displayed in Figure 4a the step velocity of both spirals for the four indicated directions was measured and step velocity ratios $V_i = v_i^{(2)}/v_i^{(1)}$ were calculated, giving for $V_{<2\bar{1}1>} = 1.2 \pm 0.1$, $V_{<\bar{2}1\bar{1}>} = 1.1 \pm 0.1$, $V_{<\bar{2}1\bar{1}>} = 1.1 \pm 0.1$, and $V_{<21\bar{1}>} = 1.2 \pm 0.1$. This indicates that step velocity is step height independent or that the interstep spacing of the two steps of spiral 2 is greater than the typical width of the diffusion fields for steps.

To ascertain the presence of any step−step interaction, the step velocity dependence on step spacing was determined using AFM at 298 K (Figure 4b). If the interstep distance becomes smaller than the mean free path of the admolecules, steps will compete with each other for material supply and step retardation sets in. No mutual step retardation was observed for interstep distances as low as 70 nm, indicating that the characteristic length of the diffusion fields of the steps is ≤35 nm, or 3−4 lattice parameters. Evidence for step−step interaction was found, however, in the lateral growth rate of macrosteps produced by three-dimensional clusters which adsorbed on the surface (Figure 5). From 40 different velocity measurements of the edges of macrosteps and the isolated steps on the clusters top, a 10 ± 6% decrease in lateral growth rate was measured for the tangential advancement of the 3D clusters. This is a strong indication for step diffusion field overlap. Although a direct measurement of the cluster height is not possible with LCM-DIM, the height could be determined roughly by careful counting of the number of steps required to bury the cluster. Combined with the measurement of the edge thickness, the interstep distance for the clusters edges was estimated to be on the order of 30−60 nm, well below the interstep distances sampled in the AFM experiments. We also note that the macrosteps showed temporal stability in all four crystallographic directions. Such stability can be explained in terms of mutual acceleration of steps as a consequence of surface adsorbed impurities inhibiting growth. For this mechanism, the dependence of the kinetic coefficient $b(p)$ on the slope p is expected to have a section with a positive curvature[33] ($\partial^2 b/\partial^2 p > 0$). No such curvature is observed for glucose isomerase[41] (see Supporting Information), thereby excluding step pinning as a macrostep stability mechanism. Solution flow along the direction of step motion inhibiting step homogenization[42] can also be ruled out on a qualitative basis given that macrostep stability is direction independent.

The observations above can be explained by two possible scenarios: (i) step growth rate is determined by bulk diffusion.

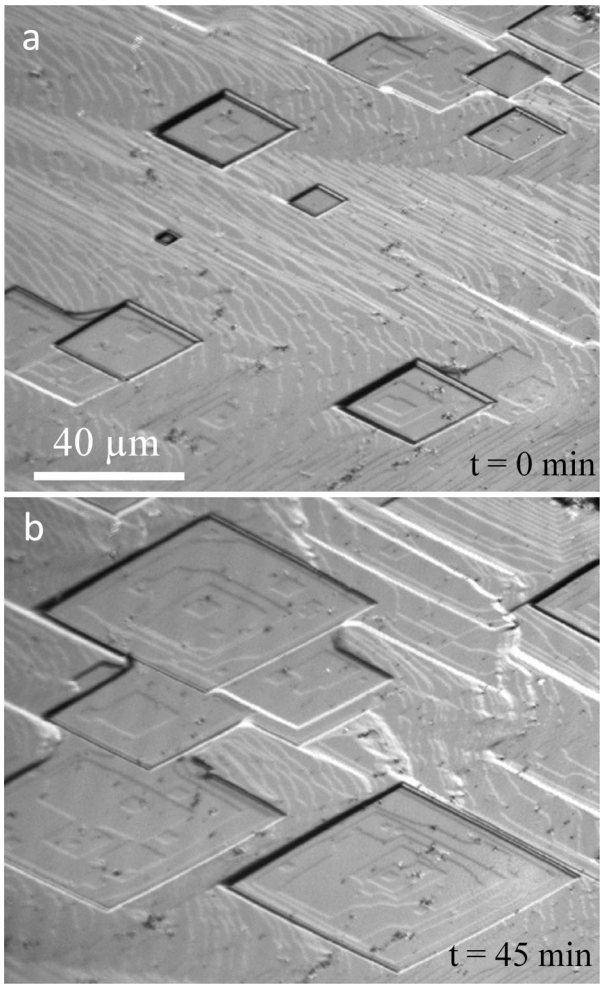

Figure 5. The lateral expansion of three-dimensional clusters adsorbed on the (011) face, between 0 min (a) and 45 min (b). The macrosteps are stable as a function of time for all four edge directions and advance slower than the steps of the newly formed 2D islands on the clusters surface.

In this case the step velocity of a double height step (for which $h \simeq D/\beta$) would reduce by a factor $(1 + \beta_{step}2h/D)^{-1} = (1 + 0.0016)^{-1}$, that is, negligible, whereas retardation of steps of macroscopic height would occur; or (ii) steps are fed through surface diffusion with an appreciable Ehrlich-Schwoebel barrier for incorporation from the lower terrace. Let us evaluate both possible scenarios using the expression for the relative velocity v/v_∞ of parallel equidistant steps controlled by either bulk or surface diffusion:[43]

$$\frac{v}{v_\infty} = \left(1 + \frac{\beta h}{\pi D} \ln\left[\frac{\lambda}{h} \sinh\left(\frac{\pi\delta}{\lambda}\right)\right]\right)^{-1} \text{ (bulk diffusion)} \tag{8a}$$

$$\frac{v}{v_\infty} = \frac{\tanh(\lambda/\lambda_s)}{1 + \frac{D_{sd}}{\beta\lambda_s}\tanh(\lambda/\lambda_s)} \text{ (surface diffusion)} \tag{8b}$$

where v_∞ is the velocity of an isolated step, λ is the interstep distance, δ is the distance normal to the surface for which $C = C_{bulk}$, λ_s is the surface distance normal to the step for which the admolecule concentration has reached the equilibrium value and D_{sd} is the surface diffusivity. As fitting parameters we used $\lambda_s = 35$ nm, $D = 3.5 \times 10^{-7}$ cm^2/s, and $\beta = 3.8 \times 10^{-4}$ cm/s. Both models predict experimental observations in a satisfactory way (Figure 4b). However, the fit based on the bulk diffusion model does require δ to be $\sim$2.5 μm. A strong deviation from the experimental data is already observed for a slightly larger value, that is, 10 μm. Given that δ is in the range of 150 μm for lysozyme[44] (with comparable values[45] for $\beta = (2-3) \times 10^{-4}$ cm/s and $D = 7.3 \times 10^{-7}$cm^2/s) a value of $\delta = 2.5$ μm would seem improbable, thereby negating the bulk diffusion model for the case presented in this work, that is, glucose isomerase. Adequate correspondence between the step velocity data and the surface diffusion model is obtained for surface diffusivities $D_{sd} < 10^{-11}$ cm^2/s. Recent single-molecule visualization experiments have estimated the surface diffusivity of fluorescence labeled lysozyme to be 4−5 orders of magnitude smaller than the bulk diffusivity.[13] This makes the obtained value of the surface diffusivity for glucose isomerase probable. Hence we conclude that for the conditions sampled in this study, surface diffusion is the dominating mass transfer pathway from the bulk toward the kink.

The Total Activation Energy for a Growth Unit En Route from the Bulk to a Kink is <22.4 kJ mol^{-1}. To investigate the temperature dependence of step incorporation kinetics, step velocities for the $< 21\bar{1} >$ direction as a function of $C - C_e$ were measured for three different temperatures 288, 298, and 308 K (Figure 6a). Care was taken to select crystals smaller than 100 μm to minimize the presence of surface concentration gradients. Additionally, step velocities were measured of steps closest to the edges or vertices of the crystal face to obtain the closest approximation of the surface concentration to the bulk concentration. Typical interstep distances were far greater than 70 nm. Using coolant flows, the temperature of the experimental cell was maintained at 1 K accuracy. The corresponding step kinetic coefficients based on the slopes of the linear fits are $\beta_{<21\bar{1}>}^{288K} = 2.9 \pm 0.1 \times 10^{-4}$ cm/s, $\beta_{<21\bar{1}>}^{298K} = 3.8 \pm 0.1 \times 10^{-4}$ cm/s, and $\beta_{<21\bar{1}>}^{308K} = 5.1 \pm 0.3 \times 10^{-4}$ cm/s. A clear acceleration of kinetics is observed. The height of the net energy barrier that molecules encounter from bulk to the step and/or kink can be ascertained by using the expression for the step kinetic coefficient for crystallization in solution. For this we use a diffusion-limited kinetics model with a mass-independent β_{step} derived by Petsev et al.[46]

$$\beta_{step} = \frac{1}{\bar{n}_k}\frac{D}{\Lambda}\exp\left(-\frac{U_{max}}{kT}\right) = \frac{1}{1 + 0.5\exp\left(\frac{w}{kT}\right)}\frac{D_0}{\Lambda}\exp\left(-\frac{U_{max} + E_{visc}}{kT}\right) \tag{9}$$

where $\bar{n}_k^{-1}$ is the kink density, D is the diffusivity, k is the Boltzmann constant, Λ is the radius of curvature of the surface−molecule interaction potential around its maximum at U_{max}. As pointed out by Chen et al.[11] both $\bar{n}_k^{-1}$ and D have an exponential temperature dependence, yielding the right-hand part of eq 9. The validity of an Arrhenius-type of temperature dependence of the diffusivity has already been verified for the case of bovine serum albumin.[47] Although a slight deviation from Arrhenius behavior is observed, this departure from an exponential temperature dependence occurs at far lower temperatures than sampled in this study, suggesting that the use of the expression $D = D_0 \exp(-E_{visc}/kT)$ is justified here.

The activation barrier derived from the fit in Figure 6b thus represents a total activation barrier E_{tot} that includes the activation barriers for viscous flow E_{visc}, the energy needed for kink formation w and the barrier for incorporation into the kink U_{max} (see right-hand part of eq 9). From the previous section

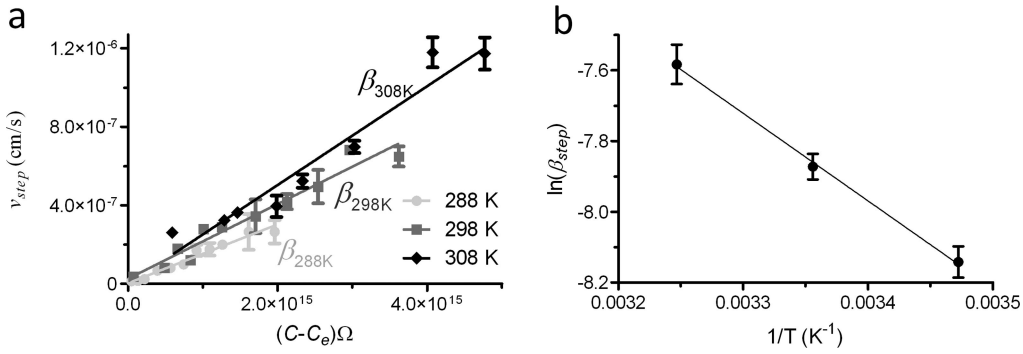

Figure 6. (a) Acceleration of step kinetics as a function of temperature. Solid lines represent fits based on $v_{step} = \Omega\beta_{step}(C - C_e)$.[34] (b) Arrhenius-van't Hoff plot of β_{step}, solid line represents fit based on eq 9.

we conclude that the growth units first undergo a partial desolvation and adhere to the crystal surface, diffuse two-dimensionally along the surface and enter the kinks after another partial desolvation. Since these elementary steps are not incorporated explicitly in the model above, eq 9 will give only an estimate of U_{max} being a function of the barriers of the individual steps involved in the surface diffusion mechanism. Nonetheless, choosing relevant approximations for the parameters in eq 9 we can get an estimate of the order of $U_{max} + E_{visc}$. Given the measured linear incorporation kinetics (Figure 2b) we consider the steps to be continuous linear sinks with respect to the admolecules and therefore $\bar{n}_k^{-1} < \lambda_s/a \approx 3.8$ giving for the kink energy $w < 4.4$ kJ mol^{-1}. Λ is of the order of a few watermolecule sizes,[46] and should therefore be in the range of 7.5 Å. The fit then yields for $U_{max} + E_{visc} = 18 \pm 0.5$ kJ mol^{-1}, which results in a total activation barrier $E_{tot} = U_{max} + E_{visc} + w$ for crystallization <22.4 kJ mol^{-1}. As a consistency check we calculate D_0 using the fitting parameters above, giving 1.7×10^{-7} cm^2/s which is in good agreement with the experimentally obtained value (using dynamic light scattering, see Supporting Information) of $(3.5 \pm 0.3) \times 10^{-7}$ cm^2/s, thereby validating the employed diffusion-limited model. The obtained value for E_{tot} is significantly smaller than the experimentally determined value for ferritin[11] and ADP,[46] that is, 41 and 27 kJ mol^{-1}, respectively.

Activation Barriers. For the case where steps are being fed by the growth units adhering to the step, the total activation barrier U_{max} en route from the bulk into the kink is determined by the barriers for adsorption U_{ad}, desorption U_{desorb}, surface diffusion U_{sd} and kink incorporation U_{kink} through $U_{max} = U_{ads} - U_{desorb} + U_{sd} + U_{kink}$. The activation energy U_{ads} for adsorption of molecules on the surface can be calculated roughly from the number of nucleation centers n_{s1} using[37] $n_s = hC_e \exp(-U_{ads}/kT)$. With C_e (298 K) $= 2 \times 10^{15}$ cm^{-3} and $h = 7 \times 10^{-7}$ cm, this yields for $U_{ads} \approx 3.8$ kJ mol^{-1}, which is surprisingly smaller compared to the value for thaumatin and ADP, that is, 13 and 11 kJ mol^{-1}, respectively. As pointed out by Malkin et al. a more extensive analysis based on the temperature dependence of n_s is required to obtain a more rigorous estimate of U_{ads}. It follows from Figure 4b that the mean displacement of the admolecules $x_s < 35$ nm. Then, through $x_s = a \exp[(U_{desorb} - U_{SD})/2kT]$[48] we obtain $U_{desorb} - U_{SD} < 7$ kJ mol^{-1}. From eq 9 the order of magnitude of U_{max} can be determined using $\beta_{step} = 3.8 \times 10^{-4}$ cm/s, $D = 3.5 \times 10^{-7}$ cm^2/s, $\Lambda = 7.5$ Å, and $\bar{n}_k^{-1} = 3.8$ giving a theoretical value of 20.1 kJ mol^{-1}, close to the experimental value $U_{max} + E_{visc}$ from the fit in Figure 6b. This gives for $U_{kink} = (20.1 - 3.8 + 7)$ kJ mol^{-1} $= 23.3$ kJ mol^{-1}. U_{max} can also be estimated from the experimentally determined value of $U_{max} + E_{visc} = 18 \pm 0.5$ kJ mol^{-1}. For aqueous polyethylene glycol (MW = 1000 Da) solutions, the activation energy for viscous flow E_{visc} is determined[49,50] to be 18 kJ mol^{-1}. This would suggest a quasi-zero barrier U_{max}. Given that this is highly improbable, the following must apply (i) there is an additional temperature dependence of β_{step} not included in the model (in eq 9) thereby underestimating the activation barrier for incorporation or (ii) the activation energy for bulk viscous flow cannot be readily utilized for the molecular surface processes described in eq 9. Additional experiments for other (model) systems should be performed to investigate this apparent discrepancy. However, we can safely conclude that, given $U_{ads} \approx 3.8$ kJ mol^{-1}, the adsorption of growth units to the terraces is not the rate-determining factor for crystallization.

Conclusion

Using in situ methods we studied the thermodynamics and kinetics of glucose isomerase crystallization. The main outcomes of this work are as follows:

(1) The solubility of glucose isomerase exhibits normal temperature dependence. The thermodynamic driving force for crystallization is the negative crystallization enthalpy $\Delta H^\circ_{cryst} = -145 \pm 7$ kJ mol^{-1} for 5% PEG 1000. The opposing entropic cost due to water/PEG trapping during incorporation into the lattice was estimated to be -380 ± 22 J mol^{-1} K^{-1} and increases for lower PEG concentrations. We attributed this diminishing of the entropy contribution at higher PEG concentrations to water structuring and a decrease in water activity.

(2) For supersaturations $\ln C/C_e > 0.7$ we have demonstrated that the prominent step generation mechanism is homogeneous 2D nucleation. At lower driving forces 2D nucleation occurs on anomalously hyperactive sites such as defects and impurity particles. The step edge free energies for homogeneous and heterogeneous nucleation are $\kappa_1 = 6.0 \pm 0.3 \times 10^{-13}$ J/m and $\kappa_2 = 2.0 \pm 0.2 \times 10^{-13}$ J/m, respectively. Furthermore, we estimate the number of nucleation centers for both mechanisms to be $n_{s1} = 3 \pm 2 \times 10^8$ cm^{-2} and $n_{s2} = n_s^* = 1.2 \pm 0.6 \times 10^4$ cm^{-2}, respectively. From the density of nucleation centers for homogeneous nucleation n_{s1} we estimate U_{ads} to be ~3.8 kJ mol^{-1}.

(3) We observed no step−step interaction for interstep distances > 70 nm. Theoretical fits of the step velocity data suggest that surface diffusion makes a non-negligble contribution to surface kinetics and is characterized by $U_{desorb} - U_{SD} < 7$ kJ mol^{-1}.

(4) A clear temperature dependence of the step kinetic coefficient β_{step} was observed. From the Arrhenius-van't Hoff

plot of β_{step} a total activation barrier for crystallization was determined to be <22.4 kJ mol^{-1}.

Acknowledgment. We are indebted to G. Nicolis and P. Vekilov for vital critical discussions. This work was supported by the Flanders Interuniversity Institute for Biotechnology (VIB), the Research Council of the VUB and the Belgian Federal Science Policy Office (DWTC). We thank the European Space Agency for financing in the context of Prodex project AO2004.

Supporting Information Available: Glucose isomerase bulk diffusivity as a function of PEG 1000 concentration, at 100 mM Hepes pH 7.0, 200 mM $MgCl_2$, and 298 K. Anisotropy of the kinetic coefficient b as a function of local slope p (•) and 4th order polynomial fit (dashed line). $\partial^2 b/\partial^2 p$ dependence on p (black line) obtained by taking the first derivative of the 4th order polynomial fit. This material is available free of charge via the Internet at http://pubs.acs.org.

References

(1) Markov, I. V. In *Crystal Growth for Beginners: Fundamentals of Nucleation, Crystal Growth and Epitaxy*; Markov, I. V., Eds.; World Scientific Publishing: Singapore, 2003.
(2) Buckley, H. E. In *Crystal Growth*; John Wiley and Sons: New York, 1951.
(3) Burton, W. K.; Cabrera, N.; Frank, F. C. *Philos. Trans. R. Soc. Lond.* **1951**, *243*, 299–358.
(4) Adam, G.; Delbruck, M. In *Structural Chemistry and Molecular Biology*; Rich, A.,Davidson, N., Eds.; Freeman: San Francisco, 1968; p 198.
(5) Berg, H. C.; Purcell, E. M. *Biophys. J.* **1977**, *20*, 193–219.
(6) Garza-López, R. A.; Bouchard, P.; Nicolis, G.; Sleutel, M.; Brzezinski, J.; Kozak, J. *J. Chem. Phys.* **2008**, 114701–114714.
(7) Vekilov, P. G.; Kuznetsov, Y.; Chernov, A. A. *J. Cryst. Growth* **1992**, *121*, 643–655.
(8) Vekilov, P. G.; Monaco, L. A.; Rosenberger, F. *J. Cryst. Growth* **1995**, *156*, 267–278.
(9) Land, T. A.; De Yoreo, J. J.; Lee, J. D. *Surf. Sci.* **1997**, *384*, 136–155.
(10) Reviakine, I. *J. Am. Chem. Soc.* **2003**, *125*, 11684–11693.
(11) Chen, K.; Vekilov, P. G. *Phys. Rev. E* **2002**, *66*, 21606−121606−5.
(12) Sleutel, M.; Vanhee, C.; Van de Weerdt, C.; Decanniere, K.; Maes, D.; Wyns, L.; Willaert, R. *Cryst. Growth Des.* **2008**, *8*, 1173–1180.
(13) Sazaki, G.; Okada, M.; Matsui, T.; Watanabe, T.; Higuchi, H.; Tsukamoto, K.; Nakajima, K. *Cryst. Growth Des.* **2008**, *8*, 2024–2031.
(14) Chernov, A. A.; Rashkovich, L. N.; Yaminski, I. V.; Gvozdev, N. V. *J. Phys.: Condens. Matter.* **1999**, *11*, 9969–9984.
(15) Carrell, H. L.; Glusker, J. P.; Burger, V.; Manfre, F.; Tritsch, D.; Biellmann, J.-F. *Proc. Natl. Acad. Sci. U. S. A.* **1989**, *86*, 4440–4444.
(16) Hill, T. L. In *An Introduction to Statistical Thermodynamics*; Bonner, F. T., Pimentel, G. C., Eds.; Dover: New York, 1986.
(17) Ross, P. D.; Minton, A. P. *J. Mol. Biol.* **1977**, *112*, 437–452.
(18) Atkins, P. In *Physical Chemistry*, 6th ed.; Freeman: New York, 1998.
(19) Tidor, B.; Karplus, M. *J. Mol. Biol.* **1994**, *238*, 405–414.
(20) Yau, S. T.; Petsev, D. N.; Thomas, B. R.; Vekilov, P. G. *J. Mol. Biol.* **2000**, *303*, 667–678.
(21) Vekilov, P. G.; Feeling-Taylor, A. R.; Yau, S. T.; Petsev, D. N. *Acta Crystallogr. D* **2002**, *D58*, 1611–1616.
(22) Koepke, J.; Scharff, E. I.; Lücke, C.; Rüterjans, H.; Fritzsch, G. *Acta Crystallogr. D* **2002**, *58*, 1757–1759.
(23) Zhang, M.; Wei, Z.; Chang, S.; Teng, M.; Gong, W. *J. Mol. Biol.* **2006**, *358*, 97–105.
(24) Hasek, J. *Z. Kristallogr. Suppl.* **2006**, *23*, 613–618.
(25) Barbosa, J. A. R. G.; Silva, L. P.; Teles, R. C. L.; Esteves, G. F.; Azevedo, R. B.; Ventura, M. M.; de Freitas, S. M. *Biophys. J.* **2007**, *92*, 1638–1650.
(26) Vekilov, P. G. *Cryst. Growth Des.* **2007**, *7*, 2796–2810.
(27) Vekilov, P. G. *Cryst. Growth Des.* **2007**, *7*, 2239–2246.
(28) Branca, C.; Magazù, S.; Maisano, G.; Migliardo, P.; Migliardo, F.; Romeo, G. *Phys. Scr.* **2002**, *66*, 175–179.
(29) Ninni, L.; Camargo, M. S.; Meirelles, A. J. A. *Thermochim. Acta* **1999**, *328*, 167–176.
(30) Suzuki, Y.; Sazaki, G.; Visuri, K.; Tamura, K.; Nakajima, K.; Yanagiya, S. *Cryst. Growth Des.* **2002**, *2*, 321–324.
(31) Sleutel, M.; Maes, D.; Wyns, L.; Willaert, R. *Cryst. Growth Des.* **2008**, accepted for publication.
(32) Sazaki, G.; Tsukamoto, K.; Yai, S.; Okada, M.; Nakajima, K. *Cryst. Growth Des.* **2005**, *5*, 1729–1735.
(33) Chernov, A. A. In *Modern Crystallography III. Crystal Growth*; Queisser, H.-J., Eds.; Springer-Verlag: Berlin, 1984.
(34) Vekilov, P. G.; Alexander, J. I. D. *Chem. Rev.* **2000**, *100*, 2061–2089.
(35) Van Driessche, A. E. S.; Sazaki, G.; Otalora, F.; Gonzalez-Rico, F. M.; Dold, P.; Tsukamoto, K.; Nakajima, K. *Cryst. Growth Des.* **2007**, *7*, 1980–1987.
(36) Malkin, A. J.; Kuznetsov, Y. G.; Glantz, W.; McPherson, A. *J. Phys. Chem.* **1996**, *100*, 11736–11743.
(37) Malkin, A. J.; Chernov, A. A.; Alexeev, I. V. *J. Cryst. Growth* **1989**, *97*, 765–769.
(38) Malkin, A. J.; Kuznetsov, Y. G.; McPherson, A. *Surf. Sci.* **1997**, *393*, 95–107.
(39) Cabrera, N.; Levine, M. M. *Philos. Mag.* **1956**, *1*, 450–458.
(40) Müller-Krumbhaar, H.; Burkhardt, T. W.; Kroll, D. M. *J. Cryst. Growth* **1977**, *38*, 13.
(41) Sleutel, M.; Willaert, R.; Wyns, L.; Maes, D. Submitted to *Crystal Growth and Design*, **2008** .
(42) Chernov, A. A.; Coriell, S. R.; Murray, B. T. *J. Cryst. Growth* **1993**, *132*, 405–413.
(43) Chernov, A. A. In *Modern Crystallography III*; Cardona, M., Fulde, P., Queisser, H.-J., Eds.; Springer-Verlag: Berlin, 1984; Chapter 5, p 209.
(44) Lin, H.; Rosenberger, F.; Alexander, J. I.; Nadarajah, A. *J. Cryst. Growth* **1995**, *151*, 153–162.
(45) Vekilov, P. G.; Rosenberger, F. *J. Cryst. Growth* **1996**, *158*, 540–551.
(46) Petsev, D. N.; Chen, K.; Gliko, O.; Vekilov, P. G. *Proc. Natl. Acad. Sci. U. S. A.* **2003**, *100*, 792–796.
(47) Placidi, M.; Cannistraro, S. *Chem. Phys. Lett.* **1999**, *310*, 130–136.
(48) Bennema, P. *J. Cryst. Growth* **1969**, *5*, 29–43.
(49) Chan, J.; Popov, J. J.; Kolisnek-Kehl, S.; Leaist, D. G. *J. Solution Chem.* **2003**, *32*, 197–214.
(50) Bai, T.-C.; Huang, C.-G.; Li, Q. *Fluid Phase Equilib.* **2003**, *207*, 209–223.

CG800756H